Rapid Fabrication of Low Impedance, 3D Dry Electrodes for Physiological Sensing

Natalie Tetreault
Ryan Kaveh

Electrical Engineering and Computer Sciences
University of California, Berkeley

December 10, 2021

Acknowledgement

Rapid Fabrication of Low Impedance, 3D Dry Electrodes for Physiological Sensing

by Natalie C. Tetreault

Research Project

Submitted to the Department of Electrical Engineering and Computer Sciences, University of California at Berkeley, in partial satisfaction of the requirements for the degree of **Master of Science, Plan II**.

Approval for the Report and Comprehensive Examination:

Committee:

Professor Ana C. Arias
Research Advisor

December 5, 2021

(Date)

* * * * * * *
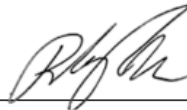
Professor Rikky Muller
Second Reader

December 9, 2021

(Date)

Rapid Fabrication of Low Impedance, 3D Dry Electrodes for Physiological Sensing

by

Natalie Tetreault

A thesis submitted in partial satisfaction of the

requirements for the degree of

Master of Science

in

Electrical Engineering and Computer Science

in the

Graduate Division

of the

University of California, Berkeley

Committee in charge:

Professor Ana C. Arias, Chair
Professor Rikky Muller

Fall 2021

Acknowledgements

Abstract

Rapid Fabrication of Low Impedance, 3D Dry Electrodes for Physiological Sensing

by

Natalie Tetreault

Master of Science in Electrical Engineering and Computer Science

University of California, Berkeley

Professor Ana C. Arias, Chair

Medical devices that record electrical activity of the human body in order to diagnose epilepsy and cardiac arrhythmias rely on a good interface between the conductors and the skin. Clinically standard devices utilize electrodes with hydrogels to reduce impedance and improve signal quality. These clinical "wet" electrodes are challenging to self-administer, which impedes the potential for in-home monitoring. Wearable dry electrodes are more practical, however they show high impedance (relative to wet electrodes). This work demonstrates a fabrication method that can produce custom shaped 3D electrodes that are optimized for each individual or specific recording location of the body. An electroless gold plating process is used in combination with 3D printing to achieve high-performance dry electrodes that do not require skin preparation and are comfortable to wear. The electrodes exhibit an average electrode-skin impedance and DC offset of 71.2 kΩ at 50Hz and 20 mV, respectively.

Contents

Chapter 1
Introduction

1.1 Motivation

Non-invasive electrophysiological (ExG) recordings such as electrocardiography (ECG), electromyography (EMG), and electroencephalography (EEG) are not only useful to physicians for diagnosing disease, but have also enabled expansive brain-machine interfaces [1], arrhythmia sensors [2], and advanced prostheses [3]. These devices typically utilize wet electrodes which require extensive skin preparation and the help of a medical professional. Wet electrodes ensure consistent and low impedance electrode-skin contact, which is essential for high signal-to-noise ratio (SNR) recordings. However, as the hydrogels dry out over time, the electrode-skin impedance (ESI) increases, causing both reduced signal amplitudes and increased susceptibility to power-line interference [4]. Additionally, the skin preparation required for wet electrodes (especially in EEG setups for sleep and epilepsy studies) often leads to skin-irritation, hair loss [5], and discomfort from residual gel left in hair.

Commercial product developers have attempted to expand these clinical techniques to everyday users by incorporating dry electrodes that are ideally placed at the wrist, limbs or forehead to transduce ECG [6], EMG [7], and EEG [8] signals. Dry electrodes increase usability and patient comfort but generally result in higher ESI (>1 MΩs at <250 Hz) relative to wet-electrodes (10-100s kΩs at <250 Hz) [9].

Several approaches to lower ESI and improve the mechanical stability of dry electrodes are discussed in the following section. For example, pin electrodes may be optimal for recording through hair while conformal electrodes can achieve higher SNR recordings in locations such as inside ear canals or around forearms [10] [11]. Ultimately, it is rare that one single technique is suitable for targeting all biopotential signals.

A wearable device that is accepted by patients for long term, repeated use must be comfortable and should not interfere with daily activities. For EEG, it is preferable to record through hair without the need for shaving, contacting gels or skin preparation. The electronic performance must not be compromised by the fabrication method or novel design, as low electrode-skin impedance and electrode DC offset (EDO) are essential for sufficient signal quality. Finally, reusability and scalable fabrication methods are also preferred.

1.2 Approaches to Dry Electrodes

Recent studies on such dry electrodes have utilized flexible planar structures, conductive composites, machined metals, or 3D-printed devices to increase electrode compliance, comfort, and freedom in sensing location [12] [13] [11]. Flexible electrode arrays often involve printing conductive inks onto a flexible plastic substrate. The advantages to this approach include high-volume fabrication and fine spatial resolution. However, flexible planar structures are limited to flexing along only one axis, such as around arms, but not on curved body parts such as an ear canal. They

also perform poorly on hairy surfaces. Dry conductive composites such as silicone carbon black and silver-glass silicone can achieve optimal electrode shapes and comfort across sensing locations, but their conductivity is still significantly worse than dry metal electrodes (for a given surface area) [14]. Some have also taken the approach of 3D printing or micromachining with conductive materials, and then depositing thin films afterward via sputtering or evaporation [15] [16]. While suitable dry electrodes for hairy surfaces can be produced this way, the designs are limited to sharp pin-like structures in order to prevent open-circuit shadows and/or non-uniform coatings. They often obtain low impedances, but do so by penetrating the upper layer of skin, which introduces risk of infection with reuse [9]. Machining and thin film deposition also tends to be costly and time consuming.

Recently, solution processed electronics have shown promise in large area, three-dimensional medical systems such as tight-fitting, radio frequency (RF) coils for improved magnetic resonance imaging [17] [18]. A more recent approach to transforming planar, printed devices has been to vacuum form them into 3D shapes. In this workflow, sheets of polycarbonate substrate were patterned with conductive silver ink by spray coating over a laser-cut design made with PET tape (Figure 1a-d). After removing the tape, the substrate is clamped in a vacuum forming machine, which heats the substrate from above until it is pliable (Figure 1e). At this point, the platform with the target mold is quickly raised and vacuum is drawn to create a tight, conformal seal (Figure 1f). Once the substrate cools (typically within seconds), the 3D shape is maintained (Figure 1g). While this approach works well for lower strain mold

designs, attempting to extrapolate this to EEG electrodes for example is challenging

for several reasons.
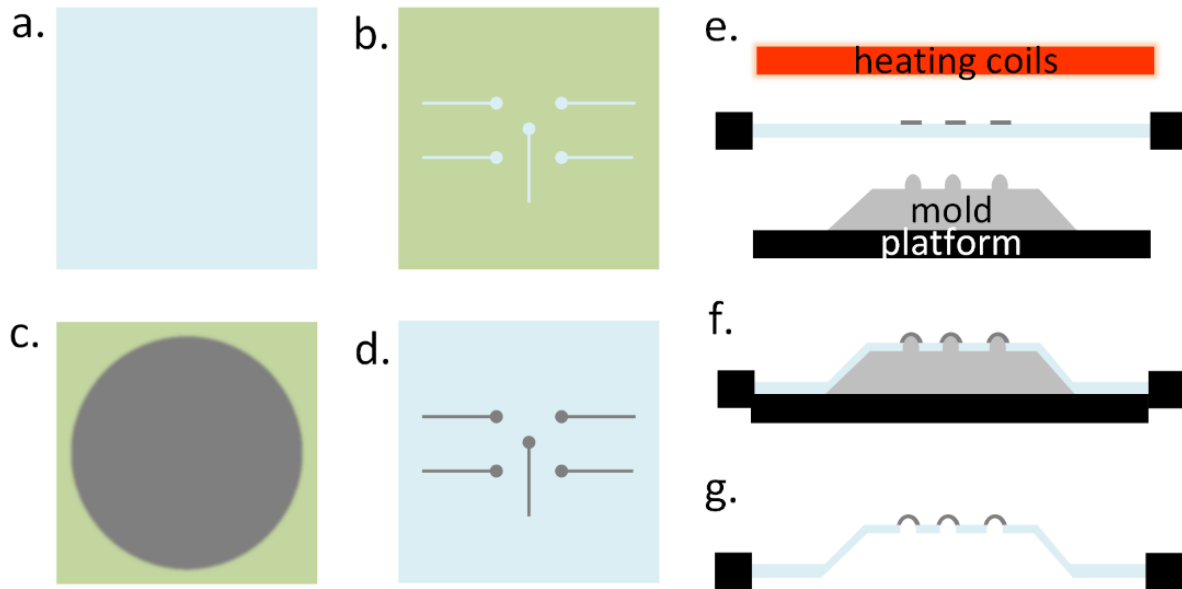
Figure 1: Printing and vacuum forming process flow. (a) Polycarbonate substrate. (b) Substrate is masked with PET tape and design is laser cut and peeled off. (c) Silver ink is deposited via airbrush. (d) Tape is peeled off. (e) Substrate is then clamped into vacuum former where it is heated from above. (f) After substrate is pliable and heating coils are pulled back, the platform with the mold is raised and vacuum is drawn. (g) The substrate quickly cools and retains its shape when the mold is removed.

First, there is the challenge of creating a planar design for printing that will

end up in the correct positions on the eventual 3D shape. This can be achieved by pre-

distorting the planar design by either manually counting coordinates after vacuum

forming a laser-etched grid pattern on a bare plastic sheet (Figure 2a), or using

computational software [19]. Along with removable alignment markers on the mold

(Figure 2b), sufficient alignment can be achieved this way on a barren substrate

(Figure 2c). However, the introduction of conductive ink reflects the heat radiated by

the vacuum former's heating coils, causing the substrate material below printed

regions to remain more rigid. This often leads to misalignment (Figure 2d) and/or

flatter structures than would be achieved with a bare, unprinted substrate (Figure

2e). Additionally, even if sufficient alignment is achieved, the inks often crack under the stress of the sharper mold shapes necessary to create devices that can penetrate through hair, which significantly lowers conductivity (Figure 2f). Additionally, this process is also limited to molds that are convex in order to prevent the substrate from getting stuck. The printing and vacuum forming process could be suitable for certain applications, such as EEG on the forehead, but to achieve good contact on hairy parts of the scalp, a different approach is needed.
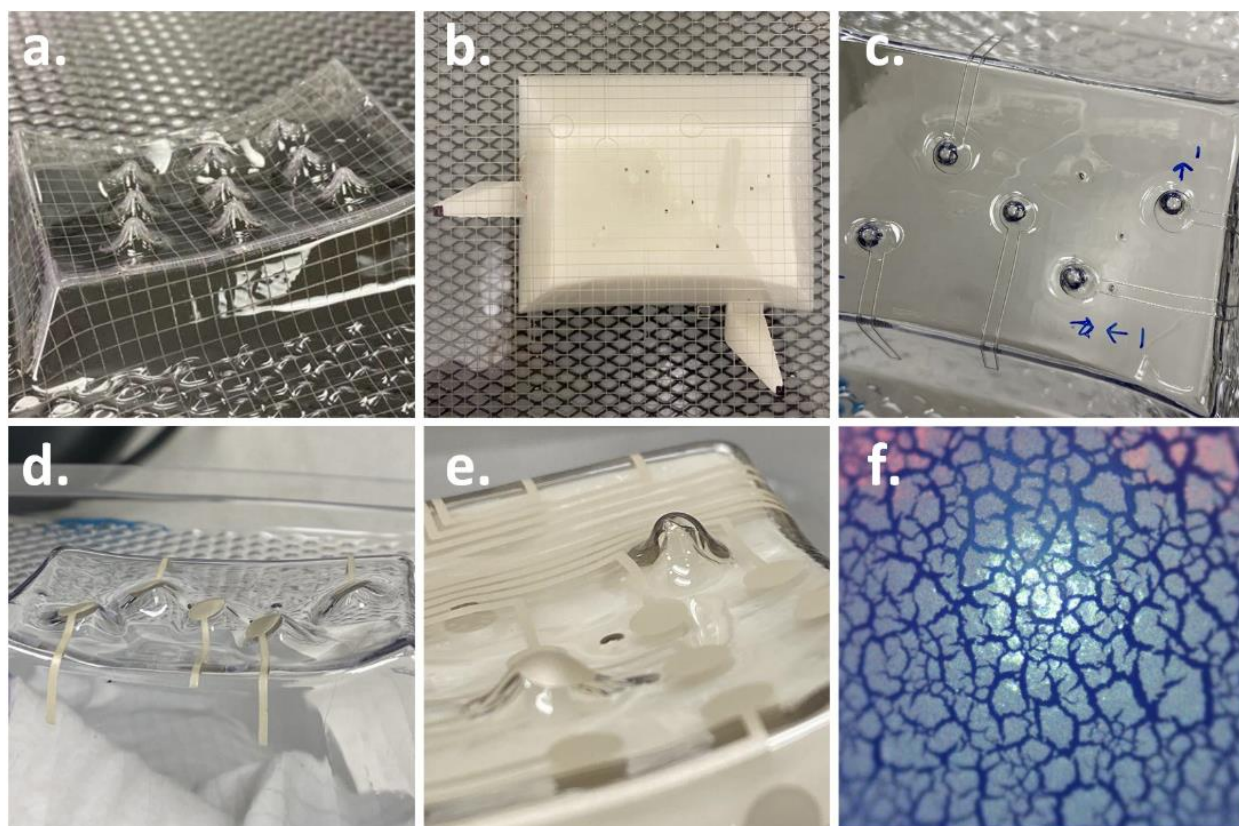
Figure 2: Challenges to printing and vacuum forming bioelectrodes. (a) Polycarbonate substrate with laser-etched grid pattern for deformation analysis. (b) Alignment mechanism comprised of removable arms in the mold whose tips lie flush with the bottom of the substrate. (c) Vacuum formed substrate with design outline etched, demonstrating sufficient alignment without any ink present. (d) A printed and vacuum formed substrate demonstrating challenges to aligning with printed designs, as the substrate underneath the printed region stays more rigid and gets pulled to one side. (e) Printed and vacuum formed substrate demonstrating the difference in shape after vacuum forming with two of the same pointed shapes on the mold. The printed region does not become as pliable and thus does not form as tightly. (f) Microscope image of cracked ink from vacuum forming.

1.3 Printing and Plating

Recently it has been shown that 3D printed parts can be electrolessly plated with a <1mm thin gold film [20]. While an excellent first step, this direct gold plating process is not ideal for wearable prototypes because the films cannot be soldered to. However, electroless copper plating processes can result in solderable, thick films on plastic parts [21]. The fabrication process presented in this work combines 3D printing with electroless copper and gold plating processes to form a multilayer stack that can easily be soldered. The process can be used to metalize 3D dry electrodes of any shape with a biocompatible gold finish and high-effective surface area.

This work showcases the benefits of this fabrication process by demonstrating different 3D printed and plated dry electrodes that are optimized for common sensing locations through hair and on fleshy skin. To record EEG, pin electrodes with bulbs on the tips were designed for optimal patient comfort (Figure 3a). To record EMG from the arm, versatile circular electrodes (Figure 3b) were integrated with flexible 3D printed wristband structures for use on a variety of arm sizes, or for use on the wrists to record ECG signals. While straightforward in nature, these proof-of-concept designs can be adapted for virtually any target location. Furthermore, they lay the groundwork necessary for fully 3D printed prosthetics with electrodes that are custom-made for each patient's unique anatomy. The electrodes not only exhibit high effective surface areas but also a durable gold plating exceeding 4 months of use. When compared to wet electrodes of the same area, they express comparable electrode-skin impedances. The results demonstrate an electrode fabrication process

that can be used to rapidly produce anatomically optimizable, low impedance, 3D dry electrodes that achieve stereotypical physiological recordings over long periods of time.
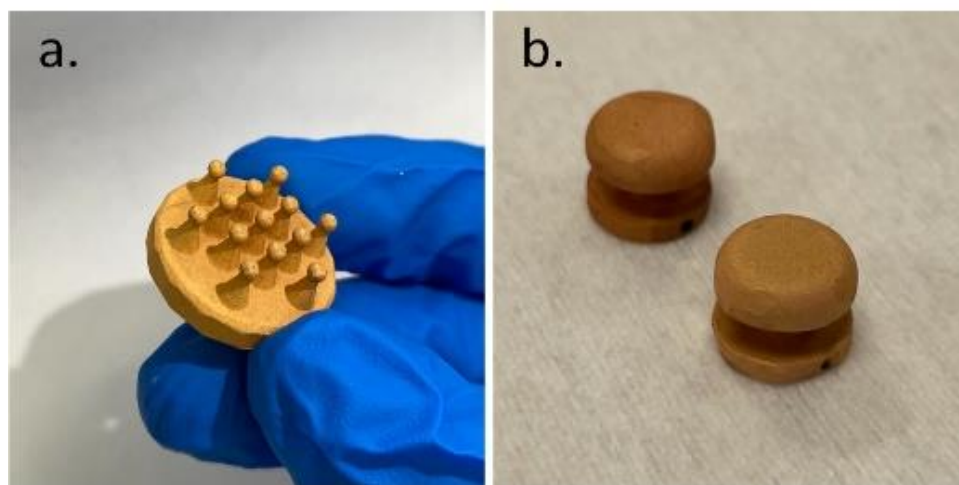
Figure 3: 3D printed and electroless plated electrodes. (a) Pin style electrodes optimized for comfortable EEG recording. (b) More general button style electrodes suitable for hairless site recordings such as EMG or ECG.

Chapter 2
Fabrication Process

2.1 3D Printing

The electrode structures were printed using a stereolithography 3D printer with a standard methacrylate photopolymer (Formlabs Form 2 Printer and Clear Resin) (Figure 4a). Stereolithographic (SLA) printers create 3D structures by precisely laser-curing photosensitive polymer resins in a layer-by-layer fashion. This method of 3D printing results in much finer resolutions and wider choices of materials than fused deposition modeling (FDM) printing, which melts and extrudes plastic filaments. After printing, the samples were post-processed with a 20-minute IPA bath to rinse away uncured resin, followed by an approximately hour-long UV curing process to fully cure the surface.

2.2 Electroless Plating

The structures were then sandblasted with 100 grit white fused aluminum oxide blasting media (Industrial Supply, Twin Falls, ID) to increase their surface area and promote better film adhesion and lower skin-electrode impedance [21] (Figure 4b). The samples were sonicated in a bath of DI water with Alconox cleaning solution for approximately 10 minutes before rinsing and sitting in a 1% benzalkonium chloride (Sigma Aldrich 12060-100G) surfactant solution for 10 minutes. These steps ensure the plating surface is clean and increases the surface energy to promote

adhesion of the catalyst. Prior to each subsequent plating step, the samples were also rinsed and dried thoroughly.

Both the catalyst and copper plating solutions were made ahead of time. A palladium-tin catalyst solution was prepared between 60-70°C and was stirred for approximately one hour after all components were added. This solution is prepared in full and lasts several weeks before the salts precipitate and it becomes no longer usable. Following the cleaning and surfactant steps, the samples were submerged in a beaker of the catalyst solution for 10 minutes, then rinsed and dried thoroughly prior to electroless copper plating.

The two main components for an electroless plating solution are a metallic salt and a reducing agent [22], in this case, copper(II) sulfate and formaldehyde respectively. At a sufficiently high pH (our solution is adjusted to 12.8 by adding NaOH), formaldehyde reacts with hydroxide ions in solution to reduce copper ions in the salt:

$$Cu^{2+} + 2HCHO + 4OH^- \rightarrow Cu + H_2 + 2H_2O + 2HCO_2^-$$
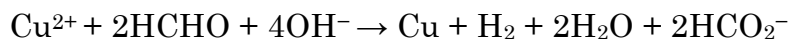
Another notable additions to the solution are EDTA, which acts as a complexing agent (as copper salts are insoluble at pH > 4), and ferrocyanide, which acts to stabilize the solution over time. The solution is stored without the addition of formaldehyde, which is then added to the appropriate quantity being used for plating when necessary. Layers are typically built at a rate of about <1μm/h at ambient temperature [22], so leaving the samples for several hours or overnight in a covered plating solution provides sufficient coverage (Figure 4c). A lightly bubbling nitrogen

line was left in the solution to provide light agitation, promote even coverage by displacing the hydrogen gas product, and to limit oxidization of the copper during the plating process.

After copper plating, electrodes are again soaked in the surfactant and catalyst solutions, then moved to the gold plating solution at about 90°C for approximately 15 minutes (Sigma Aldrich 901670-250ML) (Figure 4d). This gold plating process is self-limiting and will cease after 0.25 µm of gold has been plated. Thus, to increase the gold film thickness, further limit grain-boundary diffusion [23] and improve electrode longevity, the samples were once more placed in the same surfactant, catalyst, and gold plating solutions once more to form an additional layer of palladium and gold (Figure 4e). The increased gold thickness and multi-layer gold-palladium stack further slows down copper diffusion to the electrode surface, preventing oxidation [23]. Recipes for each solution can be found in Table 1.
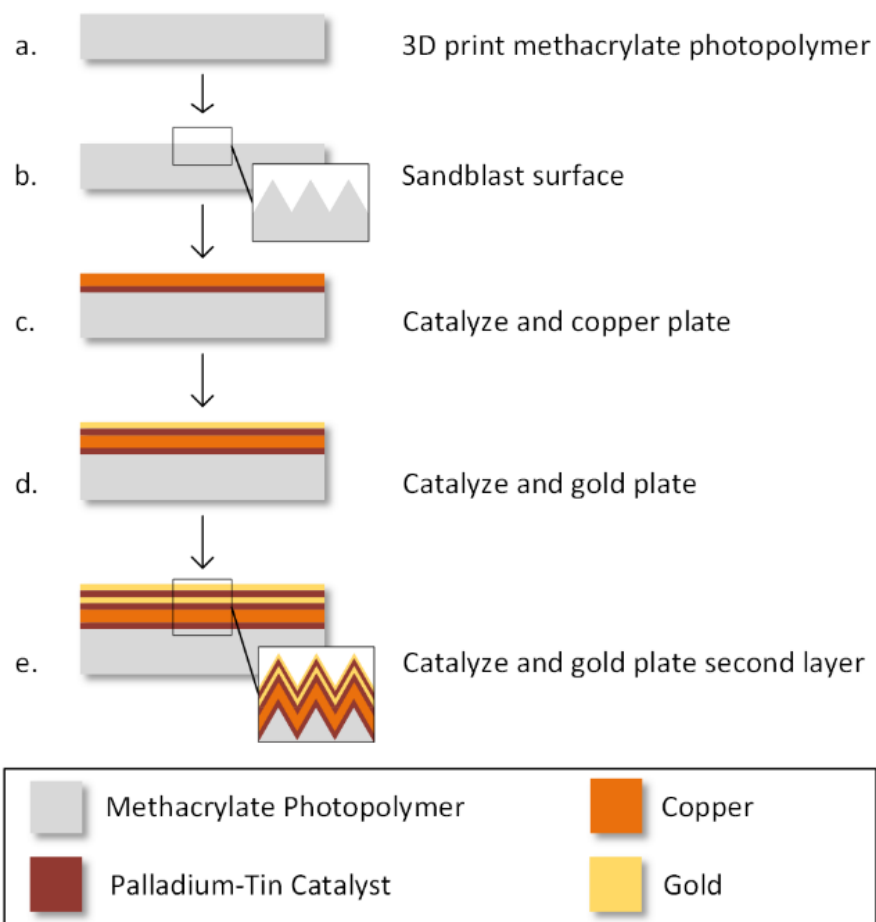
Figure 4: Fabrication process flow. (a) Design is 3D printed. (b) Sample is sandblasted, cleaned, and exposed to surfactant. (c) Catalyst, and copper plating solutions create a thick copper base. (d) Samples are submerged in surfactant, catalyst, and gold plating solutions. (e) The gold plating steps are repeated one once more for an improved diffusion barrier.

Solution	Components	Purpose
Catalyst	1 L deionized water 60 mL HCl 0.25g $PdCl_2$ 12g $SnCl_2$, after $PdCl_2$ completely dissolves	Provides very thin initial palladium layer for copper adhesion
Electroless Copper	1000 mL deionized water 18g $CuSO_4 \cdot 5H_2O$ 48g EDTA 57.2mg $K_4Fe(CN)_6 \cdot 3H_2O$ 1 mL HCl - NaOH as needed to adjust pH to 12.8 - Formaldehyde, when ready for use in 22.5:1 ratio of plating solution: formaldehyde	Plates a thick layer of highly conductive material
Electroless Gold	Bright electroless gold plating solution (Sigma-Aldrich Part Number: 901670)	Protects copper oxidation from outside environment and improves biocompatibility

Table 1: Plating process solution components and purpose. All materials were purchased from Sigma-Aldrich.

This multi-layer electroless plating fabrication technique enables the rapid prototyping of electrodes for all applications. Any electrode shape will be evenly metalized with a gold finish and result in a biocompatible dry electrode. The resultant surfaces are robust enough to be directly soldered to, which allows for simple interconnects between the electrode and ExG acquisition hardware. Lastly, this procedure has the added benefit of being performed at relatively low temperatures, thus preventing mid-process thin film thermal expansion that can lead to film flaking and peeling (a common issue with electroplating thin films).

Chapter 3
Electrode Characterization

3.1 Film Characterization

To compare the benefits of multiple gold-palladium layers, sheet resistance measurements were performed immediately after plating and once every week over the course of four weeks. Initially, copper plated samples, single layer gold samples, and double layer gold samples exhibited an average sheet resistance of 19.2 ± 1.7 mΩ/□, 17.6 ± 1.1 mΩ/□, and 16.5 ± 0.7 mΩ/□, respectively. The addition of the second layer of gold was shown to lower both the average sheet resistance of the sample as well as its standard deviation (Figure 5a), thus the samples with only 1 gold layer were subsequently eliminated from observation in the following longevity tests. After exposure to human skin and ambient air, the copper plated samples grew an oxide layer and exhibited a 20% increase in sheet resistance over the course of the test. Samples with two gold layers exhibited little visual differences over the course of the observation period and exhibited no meaningful change in sheet resistance (Figure 5b). To make a clearer comparison between samples, the sheet resistance of both the copper and gold were normalized to their respective sheet resistances on day 0.

Robust film integrity and adhesion was confirmed via tape and acid tests. To test film adhesion to the methacrylate substrate and between layers, kapton tape was applied around entire electrode surfaces and then removed. No visible gold or copper was removed with the tape, implying strong layer cohesion and film adhesion to the

substrate surface. To test for the presence of diffused copper at the surface of the electrodes, samples underwent nitric acid baths (Figure 5c). Nitric acid, a typical copper etchant, will readily dissolve copper but is not suitable for etching gold [24]. No noticeable differences were observed after dipping the samples with two layers of gold, suggesting that the gold layers sufficiently blocked etching of the copper layer. Control samples made of copper were quickly and completely etched down to the bare substrate.

The electrode-skin impedance, which is crucial to electrode performance, is inversely proportional to the effective electrode surface area. To increase the surface area without increasing the overall size of electrodes (thus lowering the density of an array) is to increase the roughness of its surface. To assess the surface roughness, light microscopy photographs were taken and stylus profilometry was performed on flat, slide-like samples of the same 3D printed photopolymer that then underwent the plating procedure (Figure 5d & Table 2). A Dektak stylus profilometer was used to collect measurements on these samples at different points in the process. Due to each plating layer being ≤ 1um thick, the surface roughness was virtually unchanged after the initial sandblasting, demonstrating that the high surface area is maintained through the metallization process.
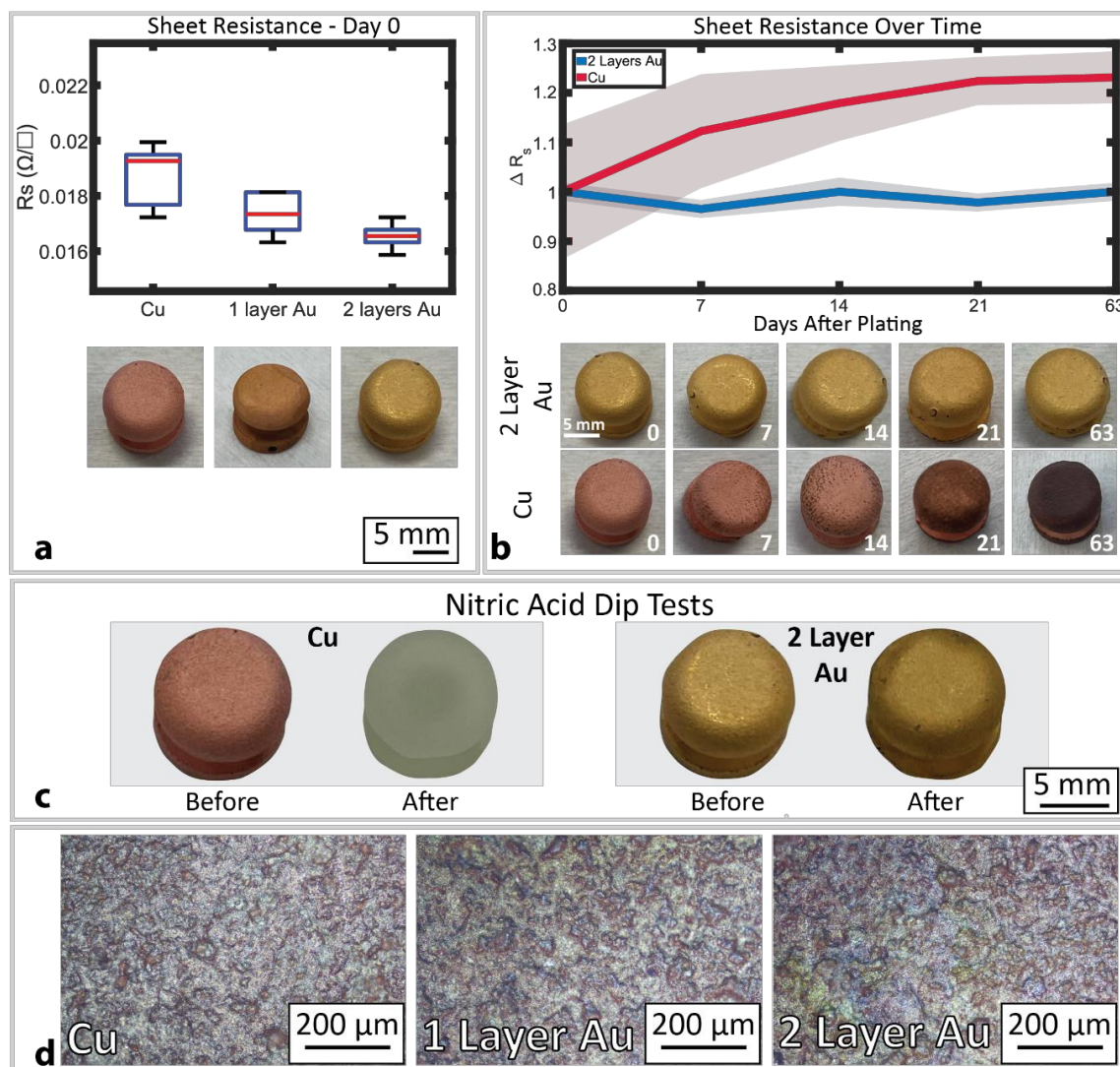
Figure 5: Electrical and physical characterizations of Au plated surfaces. (a) Box plot of absolute sheet resistance immediately after plating. In each box, the red mark indicates the median while the top and bottom of the boxes represent the 25th and 75th percentiles, respectively. The whiskers extend to the most extreme data points. (b) Sheet resistance over time normalized to day 0. Photos of the copper and copper + two layers of gold samples across the 9-week longevity study. (c) Before and after photographs of acid dip test. The copper sample was etched bare, while the double layered gold sample showed no effect. (d) Light microscopy images of plated surfaces showcasing the roughness resulting from sandblasting.

	Bare print	Sandblasted surface	Cu	1 layer Au	2 layer Au
Avg Roughness (µm)	3.34 ± 0.90	3.34 ± 0.67	4.32 ± 1.10	3.33 ± 1.19	3.50 ± 0.82

Table 2: Surface roughness at different points along the plating process.

3.2   Impedance Spectroscopy and DC Offset

Impedance spectroscopy of the 3D printed, gold-plated EEG electrodes were compared to those of standard gold cup electrodes that were filled with Ten20 conductive paste (surface area of roughly 70mm²) (Figure 6b, right). All ESI measurements were performed between two equivalent electrodes, one on the back of the head through the hair, and the other on the ipsilateral mastoid. The presented spectra in Figure 6a are half of the total measurement in order to demonstrate the impedance of a single electrode. To emulate real-world scenarios for the dry electrodes, no skin preparation was performed before each trial and measurement sessions were repeated over the course of several weeks. Gold cup electrode measurements used typical skin cleaning and preparation prior to each trial. All measurements were performed with an LCR meter (E4980 A, Keysight) and results were fit to an equivalent circuit model using a constant phase element (CPE) (Figure 6c).

While many electrode models exist within the literature, CPEs most accurately fit electrode behavior due to their ability to model the imperfect double layer formed at the electrode-skin interface [25]. CPEs are modeled by:

$$Z_{CPE} = \frac{1}{(j\omega)^n Q}$$

where $0 < n < 1$. Q is a measure of the magnitude of Z_{CPE} while n fits the bilayer phase offset. The CPE-based electrode model's total impedance, Z_{elec}, can be described by:

$$Z_{elec} = R_s + \frac{R_{ct}}{1 + (j\omega)^n Q R_{ct}}$$

where R_s is spread resistance and R_{ct} is the charge-transfer resistance.

The dry gold-plated electrodes achieved similar performance to the gold cup electrode controls when accounting for their difference in area. The dry gold-plated 3D printed electrodes (surface area of ~50mm^2) exhibited an average impedance of 71.2 kΩ and phase of -20° at 50 Hz. When a small amount of conductive paste was added, the 50 Hz impedance dropped slightly to 40 kΩ while the phase increased to -15°. Comparatively, the gold-cup electrodes (with paste) performed very similarly to the 3D printed electrodes with paste, with a 50 Hz impedance of 39 kΩ and phase of -15°. Furthermore, the gold-plated dry electrodes were stable over time. No noticeable degradation was observed in the plating finish despite heavy re-use and cleaning over the course of four months, nor did the measured impedance values increase throughout the observation period.
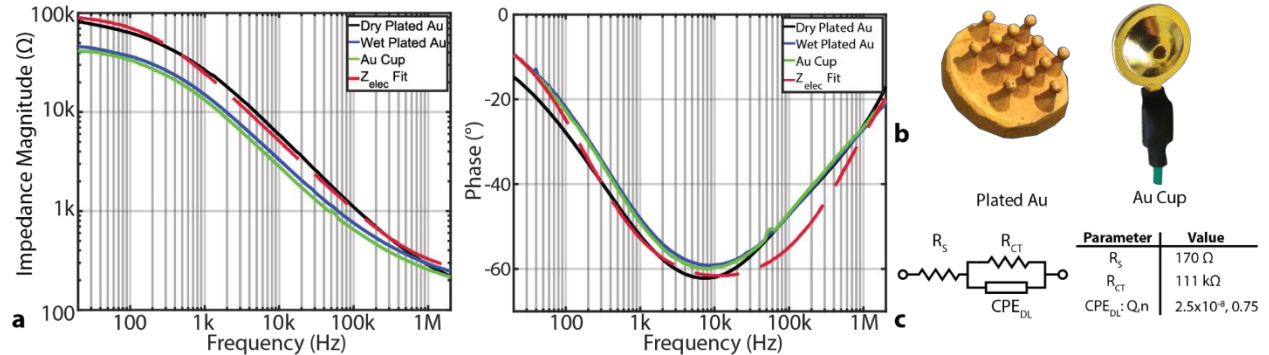
Figure 6: Electrode-skin interface (ESI) characterization of the gold-plated pin electrodes vs clinical gold cup electrodes. (a) Average (n = 5) magnitude and phase of gold-plated pin electrodes on scalp with and without electrolyte gel alongside gold cup electrodes. An electrode model with a constant phase element (CPE) model, Z_{elec} , was fitted to the dry gold-plated pin electrodes. (b) 3D-printed, gold-plated, dry EEG electrode (left) and clinical gold cup electrode (right). (c) CPE model with fitted parameters for spread resistance R_s, charge transfer resistance R_{ct}, and CPE double layer, C_{dl}.

The electrode DC offset (EDO) of the sensing electrode relative to the reference has implications on the required neural recording input range. Maintaining a low EDO keeps the recording frontend in its linear range and out of saturation.

Measurements were taken between each dry sensing electrode and an equivalently sized dry reference electrode with the WANDmini wireless recording frontend device (see Chapter 4.1) supporting a 400 mV input range and an input impedance of 40 MΩ. No skin cleaning or abrasion was performed. The mean EDO and standard deviation were -20mV ± 10 mV. The minimum and maximum EDO values were −32 mV and 23 mV, respectively. It is important to note that the measured EDO is not equivalent to the electrode's open-circuit potential due to the finite input impedance of the recording front end. Ultimately, the dry electrodes achieve low electrode impedances at frequencies of interest for ExG recordings (0-1 kHz) and maintain EDOs within the input range of state-of-the-art recording front ends [26] [27].

Chapter 4

Use Cases

4.1 Experimental Setup and Hardware

To showcase the practical feasibility of our electrodes for biopotential monitoring, ECG, EMG, and EEG signals were recorded using the WANDmini system, a low-profile, custom neural recording system that streams recorded data over Bluetooth Low Energy (BLE) to a base station connected to a laptop [10]. WANDmini is derived from a previous design for a wireless, artifact-free neuromodulation device (WAND) [28], reduced to a form factor of 2.5×2.5 cm^2, and embedded with custom firmware (Figure 7). Recording and digitization are performed by a custom neuromodulation IC [26] (NMIC, Cortera Neurotechnologies, Inc.) integrated with 64 digitizing frontends, thereby expandable to recording applications with higher electrode counts. NMIC and WANDmini specifications are listed in Table 3.
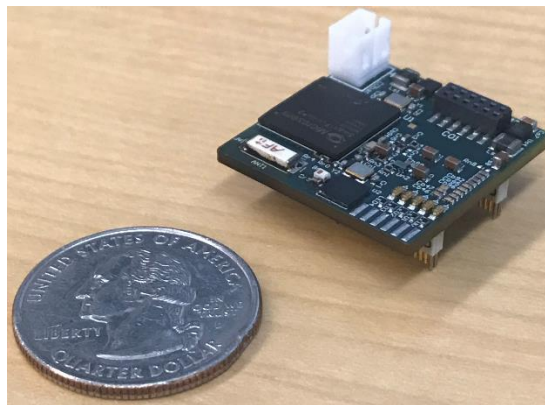
Figure 7: WANDmini neural recording device.

The NMIC was selected for its low power and high dynamic range, supporting a 100–400 mV input range with a flat input referred noise voltage spectrum of 70 nV/√Hz. The analog-to-digital converters (ADCs) have a resolution of 15 bits and sample at 1 kSps, providing sufficient resolution and bandwidth for EMG, ECG, and EEG signals. The wide linear input range can accommodate the large electrode DC offsets and provides robustness to interference.

NMIC and WANDmini Specifications	
Max Recording Channels	64
Input Range	100 – 400 mV
Input referred noise voltage spectrum	70 nV/√ Hz
Input Impedance	40 MΩ
ADC Resolution	15 bits
ADC Sample Rate	1 kS/s
Wireless Data Rate	2 Mbps
Board Dimensions	25.4 mm x 25.4 mm

Table 3: WANDmini specifications.

Each recording setup made use of 3D electrodes designed for their respective sensing locations. To mimic realistic day-to-day scenarios, no skin preparation was performed prior to electrode donning in all experiments. All subjects reported that the electrodes were comfortable to wear and none experienced any skin irritation. The user study was approved by UC Berkeley's Institutional Review Board (CPHS protocol ID: 2018-09-11395).

4.2 ECG

To record ECG, a cross body measurement was performed using 3-electrode armbands made of flexible, 3D printed material with embedded curved electrodes on each arm. Differential measurements were taken across both arm bands to record a cross-body ECG. One of the dry electrodes was selected as a ground to reduce interference in the recordings. Clear PQRST complexes were recorded and can be seen in Figure 8, demonstrating the potential to possibly detect cardiac arrhythmias.
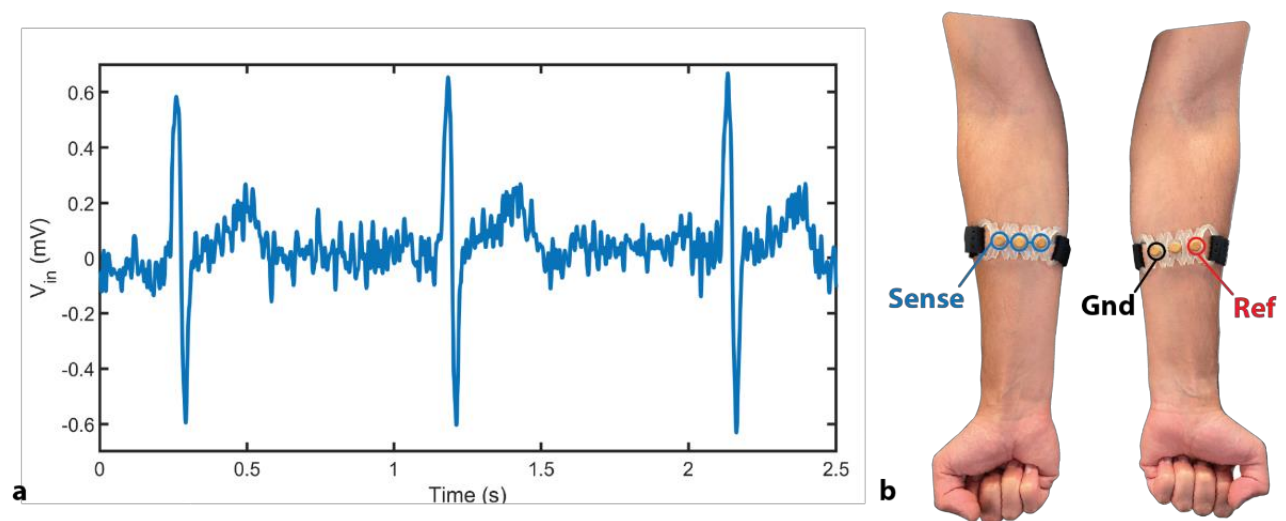
Figure 8: Electrocardiogram. (a) Time domain measurement of single lead, cross-body ECG measurement. (b) ECG measurement set up with 3D-printed bands equipped with dry electrodes on each arm.

4.3 EMG

For EMG recordings, a subject wore two bands on a single arm, one across the bicep and another by the elbow. The elbow electrodes were used as both a system ground and as references for the bicep electrodes. Sensing electrodes were placed along the bicep. Users were cued to flex their biceps every 5 seconds. Figure 9

showcases a clear increase in broad spectrum activity (0-200 Hz) both in the frequency and time domain.
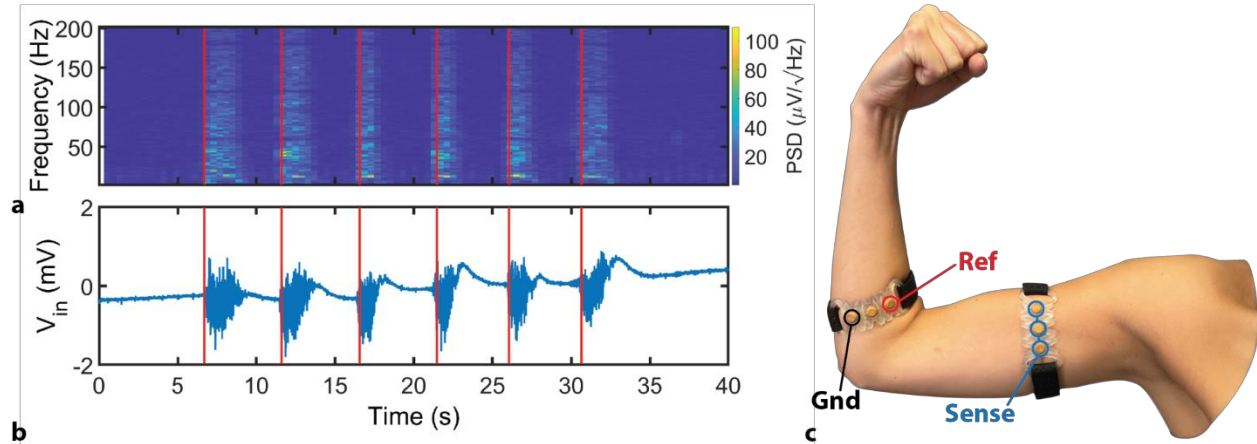
Figure 9: Electromyography. (a) Spectrogram and (b) time-domain of EMG measurements taken with two electrode bands (c) placed along a single subject's arm. The subject was cued to flex their bicep every 5 seconds. Characteristic broad spectrum muscle activity (~0 - 200 Hz) was observed when the user was cued to flex.

4.4 EEG

To record EEG through hair and oil, pin-style electrodes were placed in a flexible 3D printed headband across the head at locations T3 and T4 (according to traditional the 10-20 setup). A wet ground electrode was placed on the subject's left mastoid for interference reduction. When the subject closed their eyes, clear up-modulation of alpha band activity (8-12 Hz) was observed while lower frequency EOG activity decreases (Figure 10a). The EEG experiment was repeated on the same user with clinical gold cup electrodes with Ten20 conductive paste, placed in the same locations. The results showed comparable performance between the wet and dry electrodes. Both wet and dry electrode setups recorded alpha modulation ratios of 5

(Figure 10b), implying demonstrating little to no loss in recorded signal degradation for steady-state neural signals.
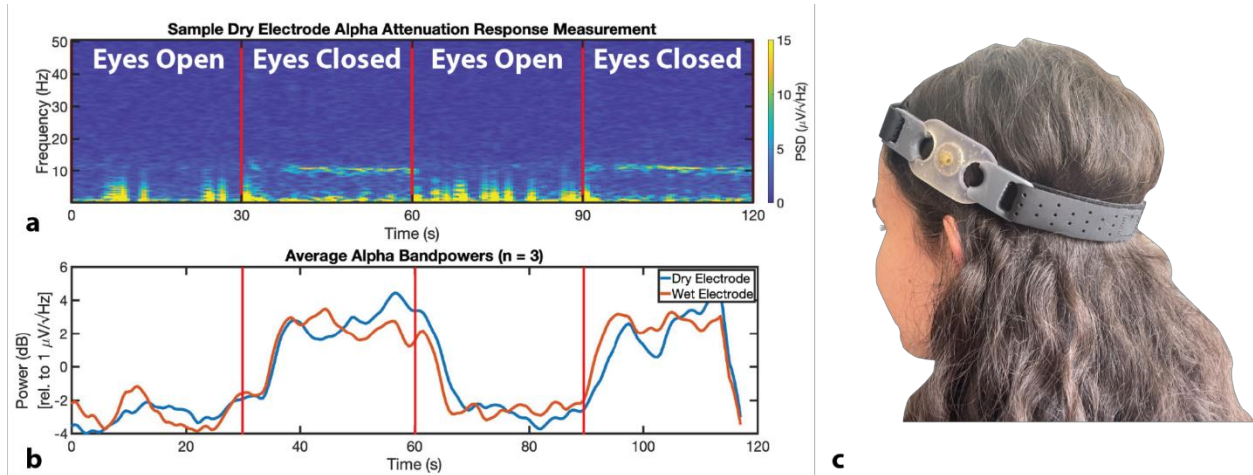
Figure 10: Electroencephalography. (a) Sample Time-frequency spectrogram of a single dry electrode alpha attenuation response. (b) Averaged (n=3) alpha (8-12 Hz) band power of alpha modulation recorded across a subject's scalp for both dry pin and wet gold cup electrode measurements. Alpha power increased by a factor of 5x in the eyes-closed state for both dry and wet measurements. (c) Alpha attenuation response measurement setup. Two dry electrodes were placed on either side of the head.

Chapter 5
Conclusion

This work demonstrates the feasibility of electroless gold plated, 3D dry electrodes of various form factors that perform similarly to wet electrodes. The fabrication process only requires a few hours of labor in addition to the 3D printing and copper plating process, and it does not involve highly expensive or complex equipment. Furthermore, due to how this technique enables anatomically fit designs, electrodes made with this process achieve electrode impedances within 10s of kΩ of clinically standard wet electrodes without any hydrogel or skin preparation, significantly increasing their ease-of-use. Lastly, these 3D electrodes can be optimized for any shape or recording location without constraints on surface feature density, overhangs, or assembly. This increased ease-of-manufacture and ease-of-use also allows for more comfortable dry electrodes, further confirming this plating process' feasibility for prototyping daily-use wearables.

To verify signal quality, different gold-plated dry electrodes were manufactured and used to record ECG, EMG, and EEG. In the case of ECG and EMG, the electrodes transduced stereotypical signals. With EEG, the alpha attenuation response recorded with the dry electrodes exhibited the same alpha modulation as the wet electrode case. As these electrodes were repeatedly used and tested over the course of four months, there was no degradation in appearance or ESI, nor any adverse skin reaction on users. Ultimately, this rapid, adaptable, and low-complexity

fabrication process results in re-usable, long lasting, and anatomically fit dry electrodes that can enable new neural wearables and devices for day-to-day health monitoring or brain-computer interfaces.

Bibliography

[1]   R. Abiri, S. Borhani, E. W. Sellers, Y. Jiang and X. Zhao, "A comprehensive review of EEG-based brain–computer interface paradigms," *Journal of Neural Engineering,* vol. 16, 2019.

[2]   Z. Ebrahimi, M. Loni, M. Daneshtalab and A. Gharehbaghi, "A review on deep learning methods for ECG arrhythmia classification," *Expert Systems with Applications: X,* vol. 7, 2020.

[3]   A. Fleming, N. Stafford, S. Huang, X. Hu, D. P. Ferris and H. Huang, "Myoelectric control of robotic lower limb prostheses: a review of electromyography interfaces, control paradigms, challenges and future directions," *Journal of Neural Engineering,* vol. 18, 2021.

[4]   E. Habibzadeh Tonekabony Shad, M. Molinas and T. Ytterdal, "Impedance and Noise of Passive and Active Dry EEG Electrodes: A Review," *IEEE Sensors Journal,* vol. 20, pp. 14565-14577, 2020.

[5]   J. Mullen and W. Morton, "Preventing Skin Breakdown in EEG Patients: Best Practice Techniques," *Journal of Pediatric Nursing,* vol. 29, no. 5, 2014.

[6]   D. R. Seshadri, B. Bittel, D. Browsky, P. Houghtaling, C. K. Drummond, M. Y. Desai and A. M. Gillinov, "Accuracy of Apple Watch for Detection of Atrial Fibrillation," *Circulation,* vol. 141, no. 8, pp. 702-703, 2020.

[7]   E. F. Melcer, M. T. Astolfi, M. Remaley, A. Berenzweig and T. Giurgica-Tiron, "CTRL-Labs: Hand Activity Estimation and Real-Time Control from Neuromuscular Signals," *Extended Abstracts of the 2018 CHI Conference on Human Factors in Computing Systems,* pp. 1-4, 2018.

[8]   A. Arsalan, M. Majid, A. R. Butt and S. M. Anwar, "Classification of Perceived Mental Stress Using A Commercially Available EEG Headband," *IEEE Journal of Biomedical and Health Informatics,* vol. 23, no. 6, pp. 2257-2264, 2019.

[9]   M. Lopez-Gordo, D. Sanchez-Morillo and F. Valle, "Dry EEG Electrodes," *Sensors,* vol. 14, pp. 12847-12870, 2014.

[10] R. Kaveh, J. Doong, A. Zhou, C. Schwendeman, K. Gopalan, F. L. Burghardt, A. C. Arias, M. M. Maharbiz and R. Muller, "Wireless User-Generic Ear EEG," *IEEE Transactions on Biomedical Circuits and Systems,* vol. 14, no. 4, pp. 727-737, 2020.

[11] A. Moin, A. Zhou, A. Rahimi, A. Menon, S. Benatti, G. Alexandrov, S. Tamakloe, J. Ting, N. Yamamoto, Y. Khan, F. Burghardt, L. Benini, A. C. Arias and J. M. Rabaey,

"A wearable biosensing system with in-sensor adaptive machine learning for hand gesture recognition," *Nature Electronics,* vol. 4, pp. 54-63, 2021.

[12] S. H. Yeon, T. Shu, H. Song, T.-H. Hsieh, J. Qiao, E. A. Rogers, S. Gutierrez-Arango, E. Israel, L. E. Freed and H. M. Herr, "Acquisition of Surface EMG Using Flexible and Low-Profile Electrodes for Lower Extremity Neuroprosthetic Control," *IEEE Transactions on Medical Robotics and Bionic,* vol. 3, no. 3, pp. 563 - 572, 2021.

[13] S. L. Swisher, M. C. Lin, A. Liao, E. J. Leeflang, Y. Khan, F. J. Pavinatto, K. Mann, A. Naujokas, D. Young, S. Roy, M. R. Harrison, A. C. Arias, V. Subramanian and M. M. Maharbiz, "Impedance sensing device enables early detection of pressure ulcers in vivo," *Nature Communications,* vol. 6, 2015.

[14] H. Dong, P. M. Matthews and Y. Guo, "A new soft material based in-the-ear EEG recording technique," in *38th Annual International Conference of the IEEE Engineering in Medicine and Biology Society*, 2016.

[15] P. Salvo, R. Raedt, E. Carrette, D. Schaubroeck, J. Vanfleteren and L. Cardon, "A 3D printed dry electrode for ECG/EEG recording," *Sensors and Actuators,* vol. 174, pp. 96-102, 2012.

[16] P. Griss, P. Enoksson, H. Tolvanen-Laakso, P. Merilainen, S. Ollmar and G. Stemme, "Micromachined electrodes for biopotential measurements," *Journal of Microelectromechanical Systems,* vol. 10, no. 1, pp. 10-16, 2001.

[17] J. R. Corea, A. M. Flynn, B. Lechêne, G. Scott, G. D. Reed, P. J. Shin, M. Lustig and A. C. Arias, "Screen-printed flexible MRI receive coils," *Nature Communications,* vol. 7, no. 1, pp. 1-7, 2016.

[18] A. Zamarayeva, K. Gopalan, J. Corea, M. Liu, K. Pang, M. Lustig and A. Arias, "Custom, spray coated receive coils for magnetic resonance imaging," *Scientific Reports,* vol. 11, no. 1, pp. 1-9, 2021.

[19] J. Ting, Y. Zhang, S. H. Yoon, J. D. Holberry and S. Ma, "iMold: Enabling Interactive Design Optimization for In-Mold Electronics," in *CHI '20: CHI Conference on Human Factors in Computing Systems*, Honolulu, 2020.

[20] S. H. Kim, J. A. Jackson, J. S. Oakdale, J.-B. Forien, J. M. Lenhardt, J.-H. Yoo, S. J. Shin, X. Lepró, B. D. Moran, C. M. Aracne-Ruddle and T. F. Baumann, "A simple, highly efficient route to electroless gold plating on complex 3D printed polyacrylate plastics," *Chemical Communications,* no. 74, p. 10463–10466, 2018.

[21] K. Gopalan, J. Maravilla, J. Mendelsohn, A. C. Arias and M. Lustig, "Vacuum Formed Coils for Magnetic Resonance Imaging," in *International Conference on Electromagnetics in Advanced Applications*, 2021.

[22] C. A. Deckert, "Electroless Copper Plating," *Plating & Surface Finishing,* pp. 48-55, 1995.

[23] S. P. Pucic, "Diffusion of copper into gold plating," in *IEEE Instrumentation and Measurement Technology Conference*, 1993.

[24] W. Pollard, "The micro-determination of gold," *Analyst,* vol. 62, pp. 597-603, 1937.

[25] W. Franks, I. Schenker, P. Schmutz and A. Hierlemann, "Impedance characterization and modeling of electrodes for biomedical applications," *IEEE Transactions on Biomedical Engineering,* vol. 52, pp. 1295-1302, 2005.

[26] B. C. Johnson, S. Gambini, I. Izyumin, A. Moin, A. Zhou, G. Alexandrov, S. R. Santacruz, J. M. Rabaey, J. M. Carmena and R. Muller, "An implantable 700μW 64-channel neuromodulation IC for simultaneous recording and stimulation with rapid artifact recovery," in *Symposium on VLSI Circuits*, 2017.

[27] H. Chandrakumar and D. Marković, "A 15.2-ENOB 5-kHz BW 4.5- μW Chopped CTΔΣ -ADC for Artifact-Tolerant Neural Recording Front Ends," *IEEE Journal of Solid-State Circuits,* vol. 53, no. 12, pp. 3470 - 3483, 2018.

[28] A. Zhou, S. R. Santacruz, B. C. Johnson, G. Alexandrov, A. Moin, F. L. Burghardt, J. M. Rabaey, J. M. Carmena and R. Muller, "A wireless and artefact-free 128-channel neuromodulation device for closed-loop stimulation and recording in non-human primates," *Nature Biomedical Engineering,* vol. 3, pp. 15-26, 2019.